RESEARCH ARTICLE

ADVANCED
NANOBIOMED
RESEARCH
Open Access

www.advnanobiomedres.com

Bioresorbable Insertion Aids for Brain Implantable Flexible Probes: A Comparative Study on Silk Fibroin, Alginate, and Disaccharides

Maria Cerezo-Sanchez, Eve McGlynn, Stefania Bartoletti, Bhavani Prasad Yalagala, Beatrice Casadei Garofani, Arianna Capodiferro, Ewan Russell, Gemma Palazzolo, Finlay Walton, Giulia Curia, and Hadi Heidari*

Miniaturized, flexible, and biocompatible neural probes have the potential to circumvent the brain's foreign body response, but the problem of surgical implantation remains. Herein, a probe intended for implantation in the rat hippocampus is coated in four bioresorbable stiffeners to determine which is most effective in aiding insertion. The stiffeners (sucrose, maltose, silk fibroin, and alginate) are evaluated through mechanical, chemical, and dissolution tests. After coating with silk fibroin, the buckling force of the neural probe increases from 0.31 to 75.99 mN. This goes in accordance with subsequent successful insertion tests. Fourier transform infrared spectroscopy results demonstrate the increase in β-sheet content of silk fibroin samples after treatment (e.g., water annealing) and show relevant changes due to dehydration of the alginate hydrogel. Both qualitative and quantitative dissolution studies in artificial cerebrospinal fluid illustrate that alginate and silk fibroin outlasts the disaccharide stiffeners. In this work, a variety of multidisciplinary analyses are carried out to find the best bioresorbable stiffener for deep brain implantable devices with the highest buckling force, longest dissolution time, and the most tunable structure. For the first time, an alginate hydrogel is used as a stiffener to aid insertion, expanding its usefulness beyond neural tissue engineering.

1. Introduction

Implantable neural devices have played a key role in neuromodulation since the earliest reports of cortical stimulation in the 1870s, the precursor to modern deep brain stimulation (DBS).[1] Although neural technology has been developed substantially in the last century, particularly during the 1950s and 60s, to treat surgical lesions,[2] it was not until the 1990s that Benabid et al. were able to showcase their work on DBS.[3,4] Their implanted electrodes combined established technologies of the time: the implantable pacemaker and nonimplantable DBS devices.[3,4]

By then, it had been two decades since the Michigan probe,[5] the first of its kind, had appeared in the literature. Investigating its design, one can see that it is a stiff, needle-like structure that laid the groundwork for countless other neural probes, and has been significantly consolidated over the years.[6] This same principle applies to the Utah array,[7] which uses a glass–silicon composite similar to the Michigan probe in terms of stiffness and was presented in the 90s. This probe has proven its efficacy in neuroprosthetics[8,9] and spinal cord stimulation.[10]

The disadvantage to these well-known neural probes is the significant glial scar they cause around the implantation site due to brain-material stiffness mismatch.[11,12] Michigan and Utah probes, made from silicon, have Young's modulus of

M. Cerezo-Sanchez, E. McGlynn, B. P. Yalagala, E. Russell, F. Walton, H. Heidari
Microelectronics Lab (meLAB)
James Watt School of Engineering
University of Glasgow
Glasgow G12 8QQ, UK
E-mail: Hadi.heidari@glasgow.ac.uk

The ORCID identification number(s) for the author(s) of this article can be found under https://doi.org/10.1002/anbr.202200117.

S. Bartoletti, B. Casadei Garofani, A. Capodiferro, G. Curia
Department of Biomedical, Metabolic and Neural Sciences
University of Modena and Reggio Emilia
Via Campi, 287, 41125 Modena, Italy

G. Palazzolo
Enhanced Regenerative Medicine
Fondazione Istituto Italiano di Tecnologia
Via Morego 30, 16163 Genova, Italy

approximately 179 GPa,[6] several orders of magnitude higher than brain tissue, which has a modulus ranging from 0.1 to 1 kPa.[13,14] To reduce the stiffness mismatch between the implantable probe and brain for long-term recording and neurostimulation, research interests have been shifting toward flexible probes.

Polymer-based probes, with substrates such as parylene-C, polydimethylsiloxane (PDMS), and polyimide, have been a topic of great interest within the literature in recent years.[15–17] These polymers have a much lower Young's modulus than silicon (in the range of 2–3 GPa). In addition, they present researchers with the advantage of higher flexibility at the time of design and fabrication compared to rigid silicon probes, as the polymer characteristics (thickness, surface modification, and fabrication methods) may be tailored to the application.

However, one key issue these flexible polymer-based probes face is their tendency to buckle at the time of insertion into brain tissue, which prevents the successful implantation of the neural probe into the brain. Researchers have tried various strategies to overcome this issue, primarily experimenting with resorbable stiffeners, shape-memory polymers, or cannula-like inserters and guides.[18–20] Resorbable stiffeners, **Figure 1**, are particularly appealing for their tuneable dissolution rate, enabling them to be tailored to the specific application, hence we focused our study on this particular set of biomaterials.[21]

Natural biomaterials are of particular significance as they typically present high biocompatibility, low immunogenicity (a key factor for implantable neural devices), and fast dissolution kinetics.[22] These can include proteins such as silk fibroin, disaccharides like maltose or sucrose, as well as longer polysaccharides like alginate. In terms of dissolution concerns, silk fibroin exhibits a degradation rate ranging from minutes to days, is adjustable depending on the concentration, and produces low antigenic by-products.[23–31] In addition, maltose and sucrose have been previously applied to polyimide probes, demonstrating an improvement in the buckling force.[32–35] Finally, alginate has been used for brain implantable biomedical devices, exploiting its highly tuneable physicomechanical properties, which allow for very low stiffness values resembling brain elasticity.[36] Still, very few studies showcase its potential as an insertion aid for neural probes, while no dissolution studies for this particular application have been reported.[37–41]

Herein, we conducted a comparative study on the performance of the four different bioresorbable coatings as insertion aids for the surgical implantation of flexible neural probes. First, we investigated their mechanical endurance by observing their bendability during insertion in both agarose models and ex vivo animal brain. Subsequently, we performed chemical characterizations on the stiffeners to evaluate how different treatments, such as water annealing or dehydration, could affect their structure and enhance their mechanical performance as a bioresorbable insertion aid. In addition, dissolution studies were conducted in artificial cerebrospinal fluid (ACSF) and in 70% ethanol to assess the dissolution rate mimicking postimplantation as well as to select the most appropriate sterilization method. Finally, a preliminary in vivo insertion test was carried out using silk fibroin as the probe coating due to its superlative mechanical performance, further described in the following sections.
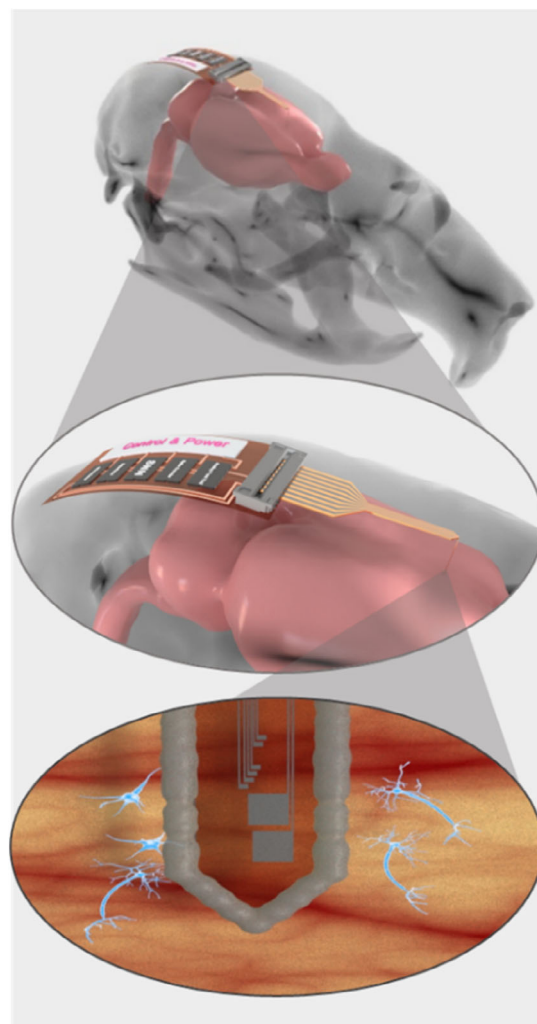
Figure 1. Schematic of the implantable flexible neural probe. Insertion of the flexible neural probe into a rat brain, showing the full system: probe, ZIF connector, and flexible PCB. Resorbable insertion aid covering the flexible neural probe.

2. Results and Discussion

2.1. Mechanical Characterization

The mechanical characterization of the bioresorbable stiffeners consisted of three separate tests to evaluate their bendability and insertion performance: buckling force tests, insertion in 0.6% agarose gel blocks, and insertion in ex vivo lamb brains.

2.1.1. Buckling Force Tests

Reducing the thickness of the probe is crucial to decrease the volume of injured tissue after insertion and increase flexibility, which may help to circumvent the foreign body response. Rather than increase the dimensions of the probe in the hope of increasing its buckling force, the argument of this work is that bioresorbable stiffeners are a much more effective method to aid insertion. As illustrated in **Figure 2**D and S3, Supporting
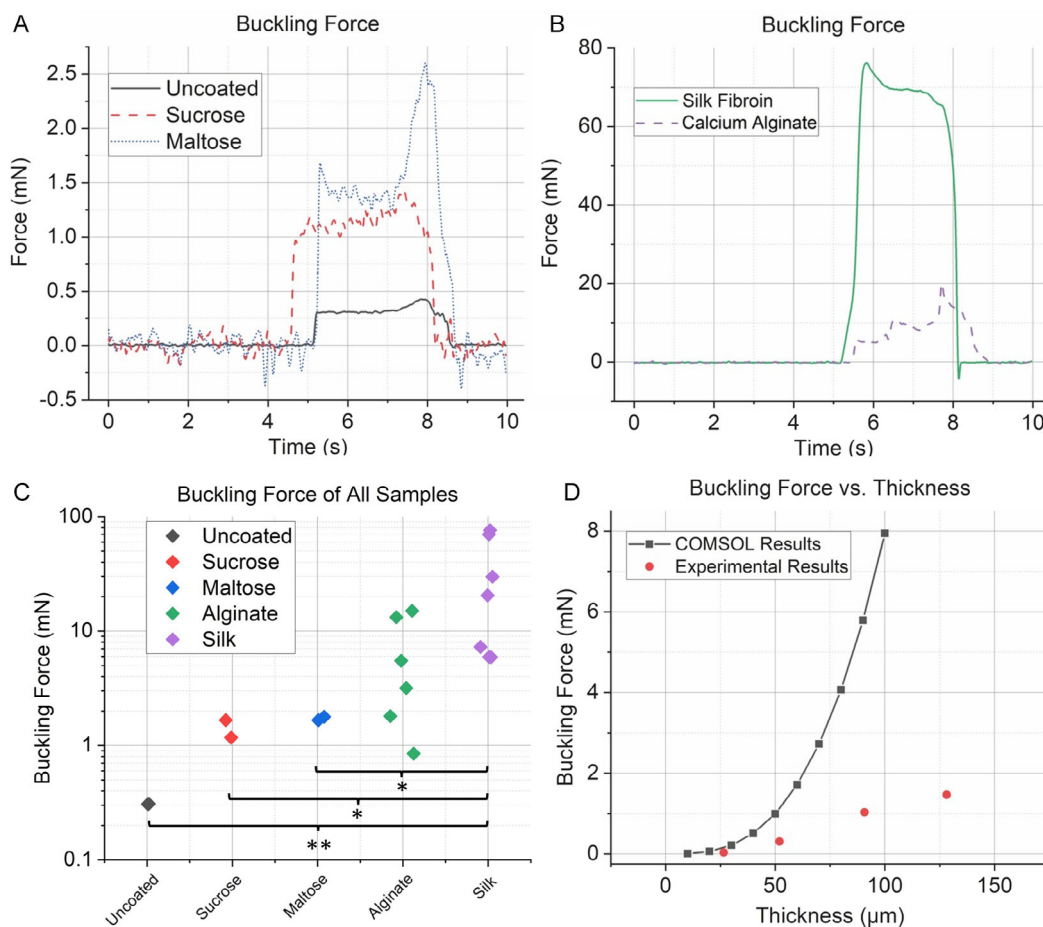
Figure 2. A) Buckling force for uncoated probes, and for sucrose- and maltose-coated probes. The "knee" which occurs after the sharp increase is the buckling force. B) Buckling force for silk fibroin- and alginate-coated probes. C) Buckling force of all samples, illustrating that the uncoated probes have the lowest critical load, with the silk fibroin-coated probes exhibiting the highest critical load. We believe that the one alginate sample which did not reach the threshold buckling force underwent delamination of the coating. One-way ANOVA with Tukey's post hoc test indicated that the silk fibroin coating produced a significantly higher buckling force compared to the uncoated probe ($p = 0.012$), to the sucrose coating ($p = 0.025$) and to the maltose coating ($p = 0.027$), while no significant difference was observed between the silk fibroin and alginate coatings; $n = 6$ for all samples (different points overlapped in the uncoated, sucrose and maltose samples due to the logarithmic scale of the graph); $*p \leq 0.05$, $**p \leq 0.01$. D) Real experimental results were compared to COMSOL Multiphysics linear buckling results. The real buckling force is much lower than the simulation results. Sample size $n = 3$.

Information, between the ≈50 μm thick probe and the ≈125 μm thick probe, there is a modest increase in buckling force of only 1.161 mN. The low buckling force of the 128.2 μm thick probe (1.467 mN) suggests that simply increasing the size of the polyimide probe to improve the probability of insertion would be unsuccessful. These results confirm the need for an insertion aid such as a bioresorbable stiffener.

For each of the bioresorbable stiffeners, various samples were tested each being named "Stiffener X" going forward. There is a strong trend in buckling force, as shown in Figure 2A,B. The uncoated 50 μm thick probes (Figure 2C) have the lowest buckling force of all the samples (0.306 mN), The sucrose and maltose coatings showcase a mild increase of the buckling force with values in the range of 1–2 mN. Alginate coatings display a further increase in buckling force up to 15 mN with an average value of 8.07 ± 7 mN. This suggests that, despite each probe coated in alginate was processed in the same way, there is a

certain level of variability impacting the mechanical properties. However, out of six different measurements, five exceeded 1 mN and only one alginate-coated sample maintained a buckling force lower than 1 mN. The oft-cited minimum value for successful implantation into rat brain tissue is 1 mN,[42] which would be possible for all coated samples, except for one of the alginate samples. Silk fibroin coatings display the highest values of buckling force, varying between 5.929 and 75.996 mN. Similar to alginate, the procedure for the silk fibroin coating was identical for each probe. The discrepancies between the buckling force of the alginate (Figure 2C) and the silk fibroin samples (Figure 2C) may be explained in four ways. First, in every case, how the probe is mounted on the universal test machine will impact its effective length, and as such, the buckling force. Second, the quality and consistency of the coating have a notable impact on the result, with delamination of coatings being a possibility (as is the case for the alginate-coated sample with a buckling force less than

1mN, which we believe to be an outlier). Third, as the coatings dry, they may shrink or curl, such that the probe is no longer straight. Fourth, the coating changes the shape of the tip, and since it is no longer strictly pointed, this changes the probe's interaction with the load cell platform. Euler's equation for a beam is appropriate for these samples, as the insertion segment of the probe is long and thin with a rectangular cross-section

$$F_{\text{buckling}} = \frac{\pi^2 EI}{(kL)^2} \qquad (1)$$

E is Young's modulus, I is the moment of inertia, k is the column effective length factor, and L is the length of the beam. Only the pointed tip deviates from this approximation; however, it is only 100 μm long, so we can consider its effect negligible. As such, the buckling force was evaluated in COMSOL Multiphysics to capture all facets of the probe shape. A beam that is not perfectly straight is not as robust and does not follow Euler's equation. For silk fibroin specifically, the variability in the resulting values may be attributed to the shape and adhesion of the silk film, as well as the effect of environmental conditions such as humidity and temperature. When the silk fibroin dries in a large, amorphous shape, the probe can no longer effectively be called a beam.

As per the equation for the moment of inertia of a beam, in which b is the width of the cross-section and h is the height of the cross-section, the buckling force increases with the cube of the probe thickness

$$I = \frac{bh^3}{12} \qquad (2)$$

However, as Figure 2D illustrates, the experimental values for buckling force display a more linear relation with the thickness, in comparison with COMSOL simulations. As the probes were mounted flat to the universal test machine with adhesive tape, and the buckling shape was observed as expected (in the forward direction, not to the left or right), it is unlikely that the experimental configuration is the reason behind the reduced buckling force. Notwithstanding, it is essential to standardize coating procedures, which is why PDMS molds and the use of laminar flow (LAF) cabinets, with temperature and humidity control, need to be part of the protocols for coating techniques. In addition to this, it should be noted that an increased sample size with tests done over a longer period of time, would benefit buckling force analysis since they would allow confirmation of the hypothesis that the experimental setup is not the reason behind the variability in the samples.

2.1.2. Insertion in 0.6% Agarose Gel

Each stiffener was further subjected to insertion tests into 0.6% agarose brain models, using both a universal test machine and surgical tweezers. As shown in **Figure 3**A, uncoated probes buckled immediately upon contact with the agarose gel block and were unable to penetrate the agarose. In contrast, silk fibroin proved to be the most successful insertion aid, with a 7 mm insertion into the agarose gel block being achieved, both using the universal test machine, shown in Figure 3B, and surgical tweezers. All other coatings showed a successful insertion with
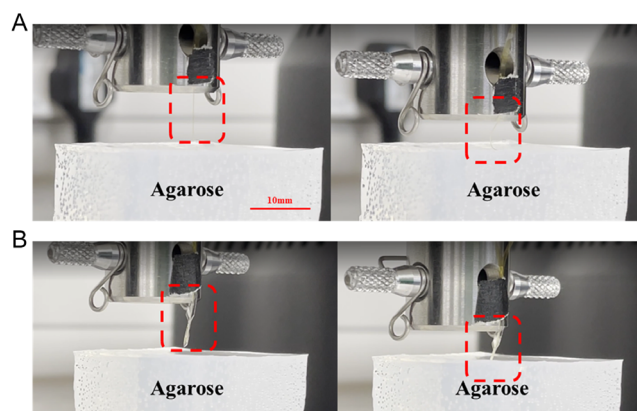
Figure 3. Insertion tests into 0.6% agarose brain models using a universal test machine. A) Uncoated probe shows buckling upon contact with surface and no insertion; B) Silk fibroin-coated probe shows no buckling and successful insertion of 7 mm into the brain model. Scale bar is 10 mm.

Table 1. Overall insertion in 0.6% agarose results for all bioresorbable stiffeners.

Stiffener Material	Universal test machine	Surgical Tweezers
Silk Fibroin	Successful	Successful
Alginate Hydrogel	Unsuccessful	Successful
Maltose	Unsuccessful	Successful
Sucrose	Unsuccessful	Successful

surgical tweezers but not with the universal test machine, as shown in **Table 1**, proving that these need a more human-controlled approach for successful implantation. In addition, delamination of the coatings was one of the main concerns, with samples like alginate showing variability in the adhesion to the polyimide substrate. Strategies like oxygen plasma etching of the polyimide could be trialed to improve adhesion in the future.[43]

2.1.3. Insertion in Ex Vivo Lamb Brain

The last mechanical characterization experiment involved insertion into ex vivo lamb brains using the same protocol as the one previously done for the 0.6% agarose gel blocks. As will be described in the Experimental Section, two different approaches were followed: a small incision of less than 5 mm in the pia mater of the brain and no incision. **Figure 4**A,B shows how even uncoated probes were able to be inserted into the brain tissue with the incision. Concerning the intact brain tissue approach, only silk fibroin probes were able to be inserted, as shown in Figure 4C,D. It was noted, however, that using the universal test machine, it was hard to achieve an optimum angle of insertion due to the unevenness of the brain surface. This had an impact on the initial buckling of the flexible neural probes and, therefore, hindered the overall performance. It was also observed that the silk fibroin sample degraded immediately upon contact with the surface of the lamb brain. The lamb brain has the advantage of presenting cerebral convolutions and helps mimic
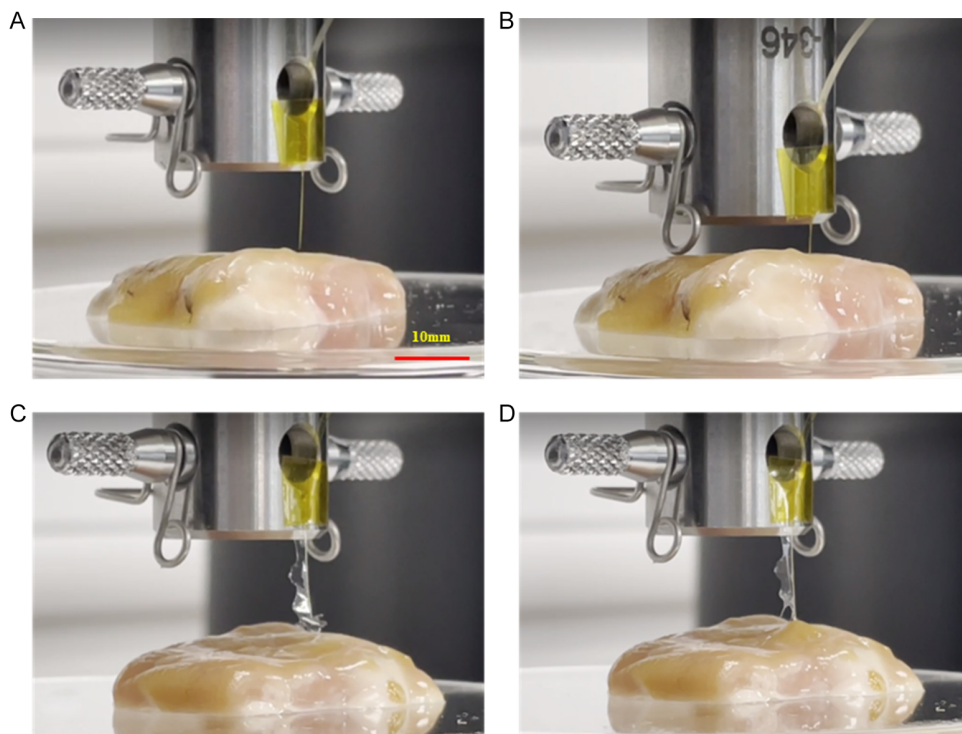
Figure 4. Ex vivo lamb brain insertion tests using a universal test machine. A,B) show an uncoated flexible neural probe being successfully inserted through a small incision in the pia mater. C,D) show a successful insertion of a silk fibroin-coated flexible neural probe through undamaged pia mater. Scale bar 10 mm.

insertion in the human brain, being, therefore, more clinically relevant than 0.6% agarose. However, being ex vivo, the lamb brain presents a reduced hydration level, lower temperature, and different texture and structure compared to the in vivo brain. To cope with this problem, we performed preliminary insertion tests in the brain of alive anesthetized rats (see 2.4 in vivo insertion section).

2.2. Chemical Characterization

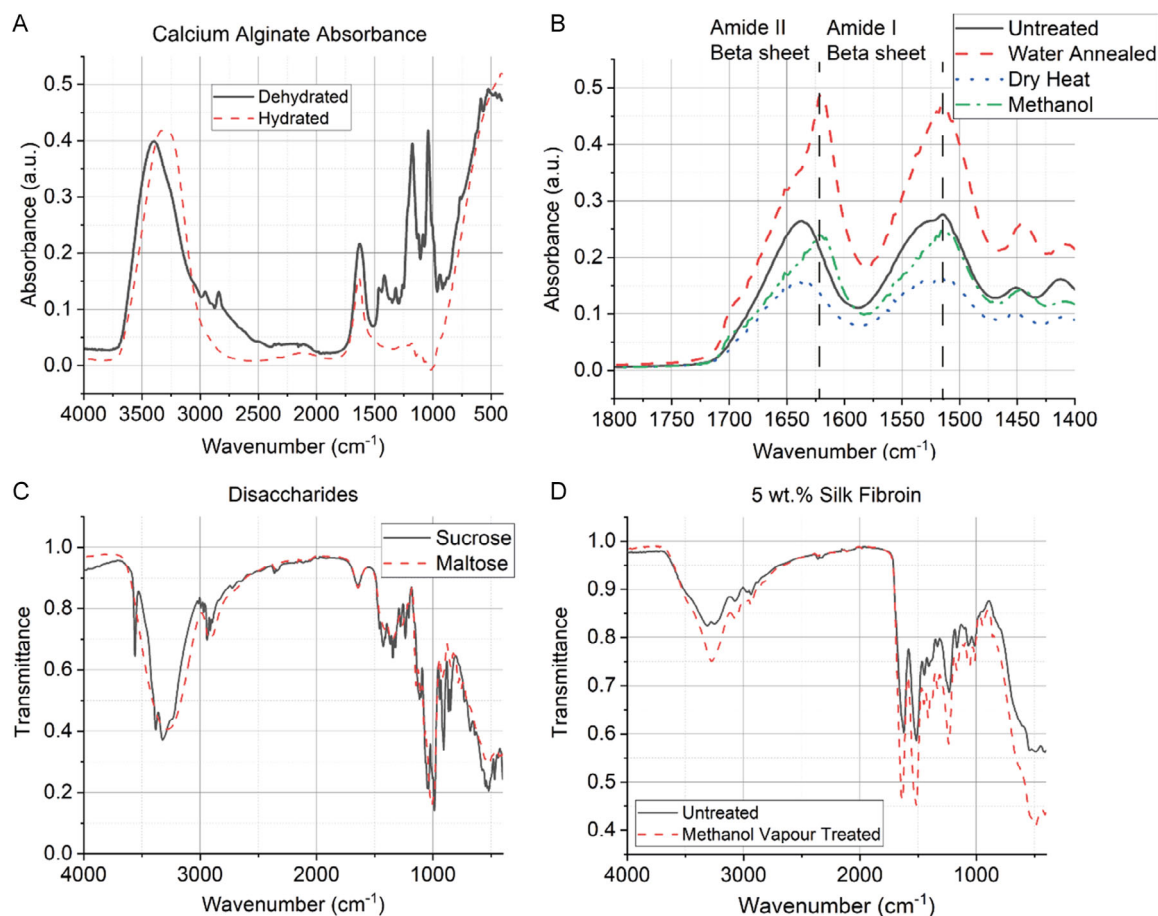### 2.2.1. Fourier Transform Infrared Spectroscopy

FTIR spectroscopy was used to characterize the stiffener biomaterials, focusing on 1) confirming the successful formation of calcium cross-linked alginate hydrogels; and 2) the analysis of the chemical changes associated with three different methods adopted to increase silk fibroin stiffness.

Sodium alginate is a linear polysaccharide extracted from brown algae, consisting of irregularly repeated units of mannuronic acid and guluronic acid.[44] Alginate hydrogel is formed by the ionic exchange of monovalent sodium with bivalent calcium ions bridging multiple polymer chains in the so-called "egg-box" structure.[45] Being the ionic cross-linking dependent on calcium, the binding kinetics and the hydrogel viscoelasticity correlate primarily to alginate macromer content and to calcium concentration.[36] **Figure 5**A shows the FTIR spectra of hydrated (red-dashed line) and dehydrated (black solid line) calcium alginate hydrogels. The hydrated sample had very high water content

and, as a result, many of the spectral features have been masked. The dehydrated sample however clearly shows bands that match data from the literature,[46,47] indicating the successful calcium-mediated cross-linking and dehydration. This includes the OH stretch band from hydroxyl groups (3500–2500 cm^{-1}), vibrations from the carboxylate salt group at 1635, 1461, and 1425 cm^{-1} and different ether groups at 1050 and 1175 cm^{-1}.

Silk fibroin is composed of polypeptide chains which form two types of ordered secondary structure, α-helices and β-sheets, both of which are held together by hydrogen bonding between the amino acids in the chains.[48] The amide groups—which are involved in the hydrogen bonds between the chains of the coils—are associated with two distinct vibrations in literature infrared (IR) data which appear at 1600–1700 cm^{-1} (Amide I) and 1500–1600 cm^{-1} (Amide II).[49,50] After the silk fibroin has been extracted—in its "untreated" form—it is mostly composed of random coils, which result in the Amide I vibration peak at 1645 cm^{-1} and a pair of faintly distinguishable overlapping peaks at 1515 and 1530 cm^{-1} in the Amide II region. Previous FTIR measurements of silk fibroin which had been treated by these methods show a strong emergent peak in the Amide I region between 1620 and 1630 cm^{-1} which has been attributed to the presence of crystalline β-sheet structures, also referred to as Silk II. It has also been observed previously that the pair of Amide II peaks go from being similar heights to favoring the lower wavenumber peak at 1515 cm^{-1}.

Our FTIR measurements of the four samples (untreated, dry heat, water annealed, and methanol vapor) are presented in

**ADVANCED
SCIENCE NEWS**

www.advancedsciencenews.com

**ADVANCED
NANOBIOMED
RESEARCH**

www.advnanobiomedres.com

Figure 5. FTIR spectroscopy results for all different bioresorbable coatings. A) Absorbance results for alginate show a significant peak at 1041 and 1176 cm^{-1} on the dehydrated sample compared to the hydrated one. B) Absorbance results for silk fibroin samples show a shift in the β-sheet peaks for the different treatments. C) Transmittance results for the disaccharides show a very similar chemical composition for both maltose and sucrose, despite some differences in their mechanical performance. D) Transmittance results for silk fibroin untreated and methanol vapor-treated samples show an increase in crystalline structure. Sample size $n \geq 2$.

Figure 5B,D. They are in agreement with the literature data,[48–50] but some show the disparity between treatment methods. The untreated sample and the dry heat-treated sample show a peak at approximately 1635 cm^{-1} in the Amide I region, with a new peak emerging at 1620 cm^{-1} as well for the methanol and water annealed samples. Similarly in the Amide II region, the untreated and dry heat samples show two overlapping peaks, but the methanol vapor and water annealed samples show a more intense vibration at 1515 cm^{-1}, with the 1530 cm^{-1} left only as a faint shoulder. The results indicate that, contrary to untreated and dry heat, methanol vapor and water annealed treatment have been more effective in increasing silk fibroin β-sheet content, enabling a decrease in the degradation rate.[51]

The FTIR data from the maltose and sucrose stiffeners are very similar, as shown by Figure 5C, owing to their similar chemical composition (both are disaccharides containing glucose—with sucrose-containing one fructose instead of a second glucose). They exhibit characteristic bands that are consistent with the literature,[52] notably the OH stretch band at 3500–2500 cm^{-1} and the ether band at 950–1200 cm^{-1}.

2.2.2. X-ray Diffraction

To further verify the crystallinity of silk fibroin (both the treated and untreated form), thin filament X-Ray diffraction (XRD) was carried out. It has been established that for Cu α XRD, diffraction peaks between 20° and 21° correspond to Silk II (β-sheets) and between 24° and 25° for what is referred to as Silk I.[53–55] Silk I is distinct from Silk II, but its crystal structure remains unclear. It is frequently reported that Silk I has a metastable crystalline or α-helical structure, but another study has concluded that it has a different β-type structure.[56] **Figure 6** shows the diffraction patterns of the untreated, water-annealed, dry heat-treated, and methanol vapor-treated samples, respectively. The untreated silk fibroin has a very broad peak around 20° which indicates a largely amorphous or random structure with a small proportion of crystalline content. In contrast, the high-intensity sharp diffraction peaks for the dry heat-treated and water-annealed samples clearly confirm that the dry heat-treated silk fibroin films have both Silk II and Silk I crystalline content. The intensity of the 20–21° peak is greater than the 24–25° peak, confirming that

2200117 (6 of 13)
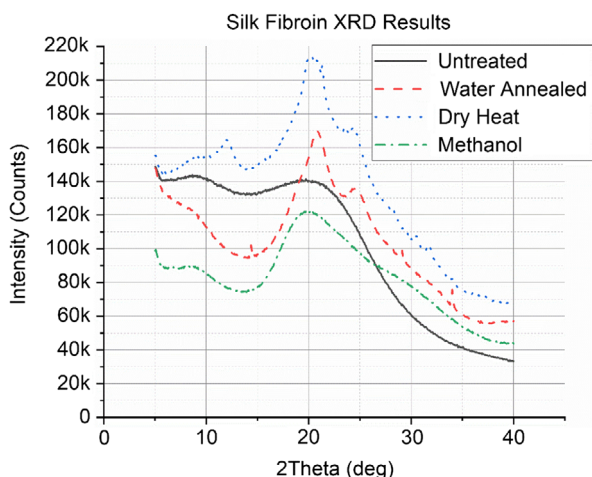
Figure 6. Silk fibroin XRD results across four different samples. Results show that the untreated sample was mainly amorphous while the treated samples, such as water-annealed and dry-heated, demonstrated a more crystalline structure. Methanol vapor-treated samples showed a peak at 20° due to the borosilicate glass substrate they were placed on. Sample size $n \geq 2$.

there is a higher fraction of Silk II content than Silk I. However, the slight shift in the diffraction peaks as compared with the dry heat-treated silk fibroin might be due to the variation in the percentage of the β-sheets. It is expected that the lesser number of β-sheets in the water vapor annealed silk fibroin might be possible as compared to the dry-treated silk fibroin films. The methanol vapor-treated silk fibroin films have less intensity with a much broader peak owing to the domination of the strong background from the amorphous borosilicate glass substrate.

2.3. Dissolution Evaluation

2.3.1. Artificial Cerebrospinal Fluid

The first dissolution evaluation was performed in ACSF at 37 °C to estimate the rate of degradation of the different bioresorbable stiffeners upon implantation. In the literature, phosphate-buffered saline (PBS) is commonly used as the testing solution;[57,58] however, it has been proven that ACSF provides a more accurate electrolytic representation of human CSF and, therefore, is more clinically relevant; in addition, ACSF can be tuned more finely.[59] In addition, the larger amount of phosphate groups in PBS can detrimentally affect calcium alginate cross-linking, through the phosphate interaction with the calcium ions leading to calcium phosphate precipitation,[60,61] dissolving the alginate hydrogel completely and hence having a significant impact on the degradation rate. In line with this, our study has also found a clear difference in the degradation rate of the samples when performed in PBS versus ACSF at body temperature, with the silk fibroin-coated samples placed in PBS degrading at a slower rate than those in ACSF (Figure 6, Supporting Information).

As shown in **Figure 7**A, the alginate hydrogel demonstrated the slowest degradation out of all samples, degrading completely between the 5- and 15 min mark in ACSF. All other samples

degraded within the first 5 min. As alginate is not recognized by mammalian enzymes, the hydrogel dissolution is mainly attributed to the chain dissociation kinetics which depends on the ionic strength and the calcium molarity of the biological fluid in which the hydrogel is submerged.[62]

It was observed that the alginate hydrogel samples experienced a rehydration process but were then more susceptible to delamination. Adhesion treatments during the fabrication process of the polyimide probes, as previously discussed in the mechanical characterization section, could help solve this issue in the future.

Regarding the disaccharides, a rapid dissolution was expected from them, given that ACSF is a water-based solution and, hence, the disaccharides are able to easily form hydrogen bonds with it and degrade it completely.[63]

It was expected that silk fibroin would showcase a full degradation within the first 10 min, as previously reported.[64] This fast degradation could be due to several factors: the low concentration of the silk fibroin (5%) and the absence of β-sheets in its structure since for this experiment we used untreated silk fibroin. Noteworthy, the advantage of silk fibroin is that it is highly tuneable, meaning that through treatments, such as the ones described in the chemical characterization section, its β-sheet content can be increased and, therefore, its degradation rate can be decreased to better fit the needs of neurosurgeons.
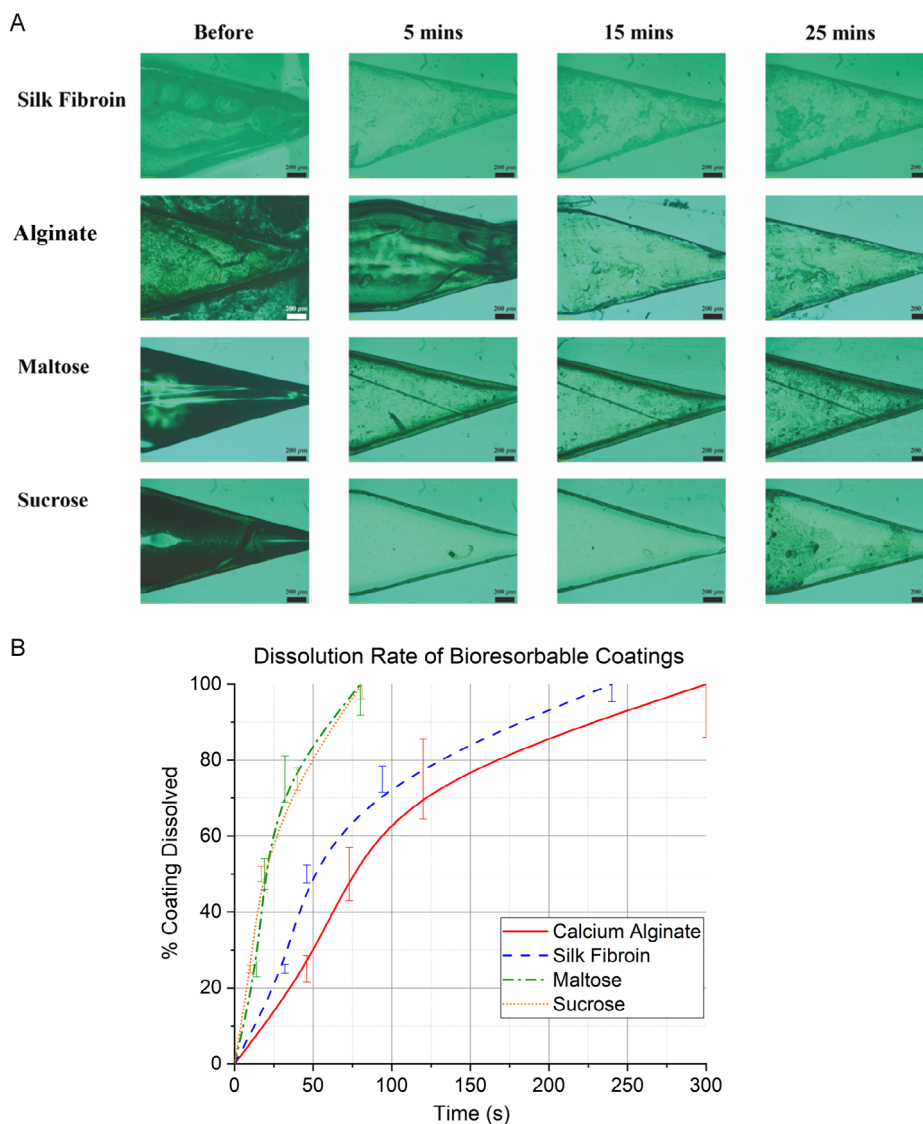
This qualitative study was followed by a quantitative analysis, further explained in the Experimental Section, examining the percentage coating dissolved over time to evaluate the dissolution rate of the four different stiffeners. As shown in Figure 7B, the four stiffeners had three notable phases in the dissolution process. The first phase showed a slower, almost linear dissolution due to the samples coming up to body temperature from room temperature. In the second phase, the dissolution accelerated very quickly while in the third and final phase, the dissolution started to slow down due to the ACSF solution becoming saturated. This quantitative analysis also supports the results obtained from the previous qualitative study, with the alginate sample dissolving at a much slower rate than silk fibroin and both disaccharides.

It should be noted, however, that this degradation is a temperature-dependent process, with higher temperatures accelerating dissolution. Studies relative to insertion probes should be strictly conducted at body temperature since samples such as silk fibroin-coated probes were shown to last in PBS for up to 25 min in preliminary studies performed at room temperature (Figure S7, Supporting Information).
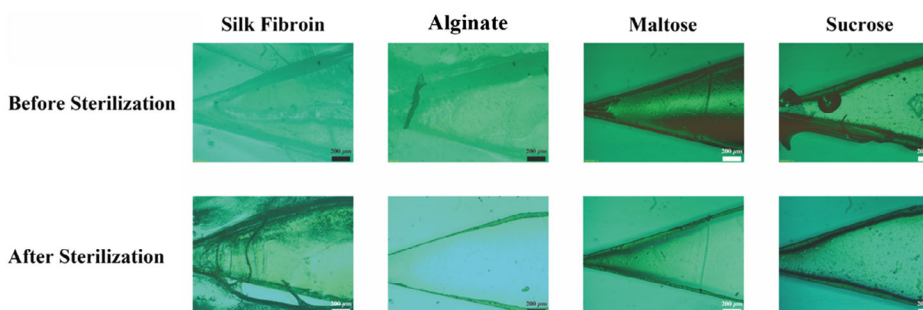
2.3.2. 70% Ethanol

The second dissolution study was done using 70% ethanol for 30 min, as shown in **Figure 8**, to evaluate the suitability of ethanol as a sterilizing agent, since it is commonly used in preclinical surgical settings due to its ease of use and availability.

It can be seen from Figure 8 that silk fibroin was able to withstand submersion in 70% ethanol for a prolonged period of time, whereas the other samples showed a complete dissolution in this solution after 30 min and, hence the need for other sterilization methods to be utilized, such as ultraviolet (UV) sterilization.

**ADVANCED
SCIENCE NEWS**

www.advancedsciencenews.com

**ADVANCED
NANOBIOMED
RESEARCH**

www.advnanobiomedres.com

Figure 7. A) Dissolution in ACSF for all four stiffeners across 25 min. Tests performed at body temperature (37 °C) show that the alginate hydrogel degrades at a slower rate than the other stiffeners due to rehydration. Scale bar is 200 μm. B) Average dissolution rate for all four stiffeners in ACSF according to the % area dissolved on HD4110 disks. The analysis goes in accordance with the qualitative results above. Sample size $n \geq 3$.

Figure 8. Dissolution in 70% ethanol for all four stiffeners; images compare probes before sterilizing treatment and after 30 min in 70% ethanol. Results illustrate the potential of this sterilization technique for silk fibroin samples, whilst other protocols should be performed for the other samples. Scale bar is 200 μm. Sample size $n \geq 3$.

**ADVANCED
SCIENCE NEWS**
www.advancedsciencenews.com

**ADVANCED
NANOBIOMED
RESEARCH**
Open Access
www.advnanobiomedres.com

2.4. In Vivo Insertion

Before in vivo implantation, dummy probes need to be properly sterilized to avoid any brain infection. In accordance with some of the results described above, sterilization of the sucrose-, alginate-, and silk fibroin-coated probes in 70% ethanol for 30 min caused the sucrose and alginate dissolution ($n = 1$ for each coating tested), and the silk fibroin coating to get a jelly-like aspect and resulted in the deformation of the probe ($n = 1$); all types of probes became unusable for the in vivo insertion (**Figure 9**A). The second approach for the probe sterilization was the use of UV light under a laminar flow hood for 30 min; with this procedure, the probes were successfully sterilized preserving their shape and characteristics ($n = 10$ for each coating tested; Figure 9B).

During the implantation (for a fully described procedure, see Experimental Section) the dummy probes were first moved close to the brain surface exposed through the craniotomy, and, with the micromanipulator on the stereotaxic frame, they were gently lowered for the insertion. The sucrose-coated probes did not enter the brain at all since sucrose dissolved as soon as it got in touch with the liquid that was keeping the surface of the brain moist[32] ($n = 0$ probes inserted out of 6 trials in 1 rat). The stiffness of the silk fibroin-coated probes was not enough due to delamination issues and the probe, within a few millimeters of the entrance, started bending (Figure 9C). It was then necessary to assist insertion using a tweezer to push the probe fully down ($n = 10$ probes inserted out of 10 trials in 3 rats), a strategy that is not convenient for in vivo preclinical studies. Furthermore, these preliminary tests showed that the alginate-coated probe could penetrate the cerebral cortex but presented bending upon deeper insertion into the brain ($n = 10$ probes inserted out of 10 trials in 3 rats); as such it was necessary to again utilize tweezers to insert the probe deeper into the brain. Due to these results, the coating methodology with

methods such as oxygen plasma treatment will be investigated to improve implantation into deep brain areas. Finally, these findings show that disaccharides such as maltose and sucrose are not good candidates for resorbable insertion aids, and that silk fibroin and alginate can penetrate the cerebral cortex but need further optimizations to reach deep brain tissue.

Hematoxylin and eosin staining performed on brain slices of the implanted rats showed that the silk and alginate probes were able to penetrate the cortex. However, they curved and did not reach the target area in the ventral hippocampus (**Figure 10**), suggesting that the coating procedure for silk fibroin and alginate needs to be revisited for in vivo applications. In addition to the suggested procedural changes, it is undoubtedly important to investigate the effect of the bioresorbable coatings on the flexible probes during the recording and stimulation of neurological activity, as well as the post-implantation inflammatory response caused by said coatings on the surrounding neural tissue. Hence, such investigations will pertain in the next stage of the research studies on these bioresorbable insertion aids.

3. Conclusion

Bioresorbable stiffeners are a novel method to solve the issue of buckling upon insertion that current implantable flexible neural probes face. In this work, we have presented an extensive study on four different bioresorbable insertion aids, demonstrating that silk fibroin is a highly tunable material, with the highest buckling force and with a degradation rate that falls within the requirements set out by neuroscientists. Other samples, such as alginate, showed promise in terms of dissolution and bendability but further adhesion studies need to be conducted on polyimide substrates. Although disaccharides such as sucrose and maltose have been reported in the literature to be acceptable bioresorbable stiffeners, we found that they show no significant increase in the buckling force, preventing indeed the probes
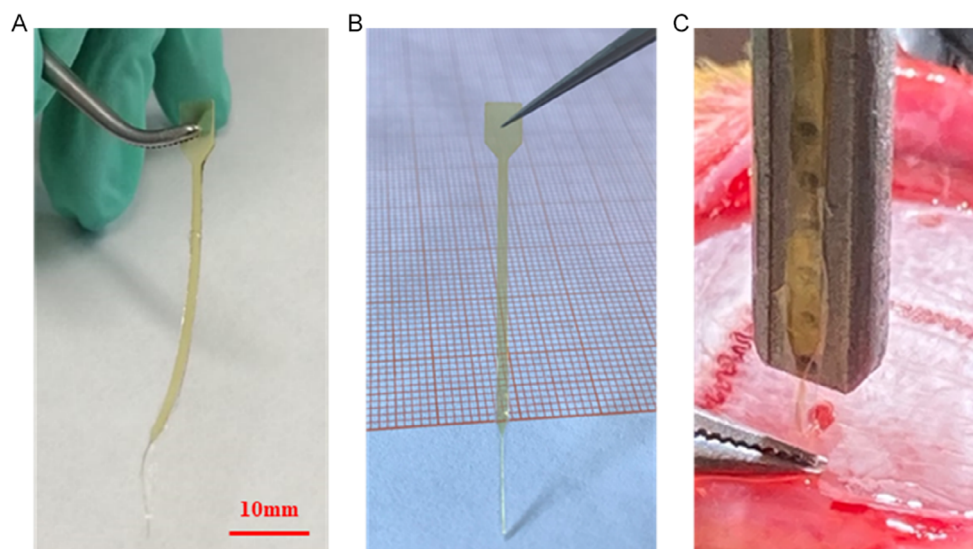
Figure 9. In vivo probe insertion. A) A silk fibroin-coated dummy probe after sterilization in 70% ethanol; the probe changed its thickness and shape. B) A silk fibroin-coated dummy probe after sterilization under UV; the probe preserved its best shape. C) Representative picture of the silk-coated dummy probe during in vivo insertion in a rat brain; note that the probe bent and was forced deep into the brain with a tweezer. Scale bar is 10 mm.
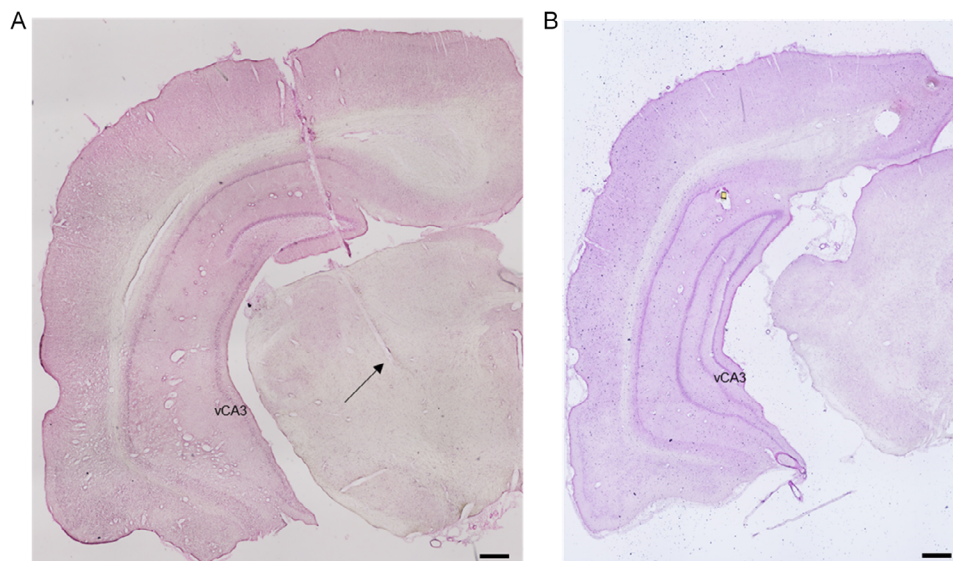
Figure 10. Ex vivo microscopy representative image of the rat brains implanted with a silk fibroin-coated probe A) and an alginate-coated probe B) after UV sterilization. Brightfield image of hematoxylin-eosin-stained brain coronal section. In violet, the cell nuclei and in pink, the brain parenchyma. (A) It is possible to clearly observe the trace left from the inserted probe. The black arrow shows the brain structure reached by the probe tip, not corresponding to the target area, the ventral CA3. (B) The probe did not reach the ventral CA3. Scale bars are 500 μm.

to be inserted into the brain. This study validates the consensus in literature over the use of silk fibroin as a bioresorbable stiffener but also presents alginate as a potential future candidate for aiding the insertion of flexible neural probes, although in both cases further optimizations to obtain accurate insertion of the probes in deep areas of the brain are needed. Notwithstanding, the findings of this study have to be seen in light of some limitations, in particular in terms of sample size and limited biological studies. As such, it is incumbent to expand such research through an increased sample size and experimental duration for the mechanical characterizations, and through the investigation of the electrophysiological signals obtained during recording and stimulation.

4. Experimental Section

Materials: The flexible neural mechanical probes were microfabricated using polyimide as the substrate. 4 inch glass wafers were solvent-cleaned using an ultrasonic bath. The cleaning process was as follows: 5 min in Opticlear solution, then acetone, then methanol, and finally in reverse osmosis (RO) water, after which the wafers were blow-dried with N_2. They were then spin-coated with PI2545 (HD Microsystems) using a PWM32 Spin Coater, soft baked at 140 °C between layers, and cured in a nitrogen oven ramped from room temperature to 300 °C for 2 h, to create what would be the release layer. After 24 h, HD4110 (HD Microsystems©) would be spin-coated onto the samples to create a 50 μm thick layer which would serve as the substrate of the flexible mechanical probe. The wafers were soft baked at 110 °C and exposed to UV using a Süss Mask Aligner, followed by a postexposure bake. Development using cyclopentanone (Sigma Aldrich CAS 120-92-3) and rinsing with propylene glycol methyl ether acetate (PGMEA) (Sigma Aldrich CAS 108-65-6) were done to develop the pattern of the probes. Finally, the samples were cured in a nitrogen oven ramped from room temperature to 300 °C for 2 h and placed in deionized water for 12 h, after which the flexible mechanical probes could be easily peeled off.

Preparation of PDMS Molds: To prepare the PDMS molds, a positive master mold out of a 4 inch silicon wafer was made, out of which the negative PDMS mold could be taken off. The silicon wafers were cleaned using a Piranha solution. Then SPR220 7.0 was spin-coated onto the wafers using a Suss RCD8 Spin Coater to create a 7.5 μm thick layer, after which they were soft-baked at 120 °C. They were exposed to UV using a Süss Mask Aligner and developed using CD-26 (Sigma Aldrich CAS 75-59-2) to develop the probes' pattern. The wafers were then dry etched using Oxford Instruments PlasmaPro Estrelas100 to create 100 μm thick, 200 μm wide probe patterns on the master mold, which were checked using a Contact Profiler Bruker Dektak XT.

PDMS was then prepared following a 10:1 ratio of PDMS (Sylgard 184) to curing agent. After being thoroughly mixed it was placed in a degasifying chamber until all bubbles were removed. The mixture was then poured onto the silicon master mold and spun coated at a low speed using an Ossila Spin Coater to create a 200 μm thick layer of PDMS. The sample was then cured at 70 °C overnight, after which the PDMS was peeled off the silicon master mold carefully with some isopropyl alcohol to avoid damage to the PDMS layer.

Synthesis of Bioresorbable Stiffener Coatings: Disaccharides: Two types of disaccharides were utilized in this study, maltose (Sigma Aldrich CAS 6363-53-7) and sucrose (Sigma Aldrich CAS 57-50-1). Regarding maltose, a 1.8% solution was made in deionized water and left to fully dissolve in a water bath at 37 °C for 2 h. Then it was placed in a hotplate at 250 °C and left there until all the water evaporated. Once a syrup-like consistency began to form, the solution was moved to the edge of the hotplate to reduce the temperature and the flexible mechanical probes were dip coated with the remaining solution.

With regards to sucrose, a 4% solution was made in deionized water and left to fully dissolve in a water bath at 37 °C for 2 h. The probes were placed in nonstick baking paper, the solution was pipetted onto the insertion zone and the samples were placed onto an oven preheated at 95 °C for 40 min until all the water evaporated and the sucrose crystallized around the probe.

Alginate hydrogel: A 2% alginate stock solution (Stock ALG) was produced by solubilizing sodium alginate (PRONOVA UP LVG) in HEPES buffer (135 mM NaCl, 20 mM HEPES, 10 mM NaOH, pH 7.47) for 24 h at room temperature. Another stock solution (Stock CA)

**ADVANCED
SCIENCE NEWS**

www.advancedsciencenews.com

**ADVANCED
NANOBIOMED
RESEARCH**
Open Access

www.advnanobiomedres.com

containing 100 mM $CaCl_2 \cdot 2H_2O$ (Sigma Aldrich CAS 10035-04-8) was prepared and, subsequently, this solution was diluted in HEPES buffer to obtain an 8 mM solution. Equal volumes of stock ALG and stock CA were mixed to obtain a final concentration of 1% alginate and 4 mM $CaCl_2$ solution. Upon mixing, the resulting solution was left to polymerize for 24 h at room temperature, covered with Parafilm to prevent dehydration. Subsequently, the gelling solution was pipetted into the PDMS molds containing the flexible mechanical probes and left to dehydrate for 24 h.

Silk fibroin and treatment protocols: 5% silk fibroin solution was purchased from Sigma Aldrich (Product No. 5154) and four different samples were prepared from it: untreated, methanol vapor treated, water vapor annealed, and dry heated solutions. The untreated silk fibroin was pipetted into the PDMS molds after the flexible mechanical probes were properly placed using deionized water through surface tension, the coatings would then be left to air-dry at room temperature for 12 h. The methanol-treated samples were spun-coated onto both silicon and borosilicate glass pieces and placed on top of a beaker containing methanol so that the vapors would be in contact with the sample. The beaker was then placed in an oven at 90 °C for 1 h. In terms of the water-annealed samples, the methodology was the same substituting the methanol for deionized water and leaving the sample in the oven for 12 h. At last, the dry heated samples were pipetted onto cured PDMS and placed on a hotplate at 75 °C for 10 min.

Mechanical Characterization: The buckling tests were performed on an Instron 5966 Universal Test Machine, coupled with a Honeywell Model 30 50 g load cell. Probes were fixed to the moving frame with tape in the same position before each test, and the height of the probe above the load cell was adjusted by the eye. The frame height was set to zero before each test such that the frame would travel the full distance in each experiment. Traveling at 1 mm s^{-1}, the probes were lowered onto a cured PDMS slice over the course of 5 s. The PDMS slice was placed on top of the load cell to prevent the probe tip from sliding during the buckling test. The results were adjusted to account for the weight of the 3D printed load cell platform and PDMS slice. The output from the load cell was monitored on an oscilloscope and saved to a.CSV file. Using the MATLAB function "smoothdata", the output was smoothed with a Gaussian filter.

0.6% agarose gel blocks were prepared as mechanical brain models,[65] by dissolving the agarose in PBS (Sigma Aldrich 806 552) under stirring at 90 °C until the solution became clear. The solution was then poured onto silicone molds and left to air-dry for 1–2 h. Tests into agarose were carried out similarly to the buckling force tests, with the exception of the load cell setup. The sensitivity of the Model 30 load cell is offset by the risk of damage when large loads above 500 mN are applied, and as such, the load cell could not be used in conjunction with heavy agarose or lamb brain. Without the load cell, the stiffeners were evaluated on a pass/fail basis, with video recordings to confirm the results of each insertion attempt. The travel distance was adjusted to 7 mm, so that in the event of successful insertion, the majority of the insertion segment would be pushed into the agarose. Two speeds were trialed: 0.5 and 1 mm s^{-1}. Finally, the insertion tests were repeated in defrosted lamb brain (Samples for Schools, UK). The pia mater was removed with a dissection kit to aid insertion. All equipment was sanitized before and after use, with 70% ethanol.

To compare the buckling force of probes with different thicknesses, first theoretical buckling force values were produced from COMSOL Multiphysics Linear Buckling simulations. A fixed constraint was applied at the point where, in reality, the probe was affixed to the Instron 5966, and a load of 1 mN was applied at the tip. Four probe thicknesses were fabricated using the same methodology as the standard 50 μm thick probes, simply by reducing the spin speed to 2000 rpm and varying the number of soft-baked layers applied before curing. Each layer added approximately 25 μm to the probe thickness, from 25 to 100 μm. The buckling force was recorded as already described.

Chemical Characterization: The different bioresorbable stiffener samples were analyzed using FTIR spectroscopy and XRD to characterize structural alterations in the samples. The FTIR spectral data for the different post-treated silk fibroin samples along with alginate, sucrose, and maltose were acquired using a Bruker (USA) Vertex 70 FTIR equipped with an attenuated

total reflectance (ATR) unit (Bruker Platinum A225). The samples were placed on the spectrometer, completely covering the diamond surface by applying pressure by the anvil of the ATR unit. Background-subtracted FTIR spectra were recorded in transmittance mode after averaging for 16 scans for a wavelength range in the mid-IR from 400 to 4000 cm^{-1} at room temperature with a resolution of 4 cm^{-1}. Next, the FTIR spectra were recorded under the absorbance mode for a short, dedicated wavenumber range of 1400–1800 cm^{-1} for the silk fibroin samples, to clearly observe the shift in the peak position in the Amide-I range (1600–1700 cm^{-1}) of treated and untreated silk fibroin films. A background scan was performed for every different sample. XRD studies were performed using a Malvern Panalytical Empyrean with PIXcel3D-Medipix3 1×1 detector using Cu Kα radiation ($L = 1.541874$ Å) in the Bragg–Brentano reflection geometry, 2-theta (q) ranging from 5 to 40° with a step size of 0.05°. XRD data were obtained for all the silk fibroin films (both treated and untreated) by placing them in a small sample holder of 5×5 mm.

Dissolution Protocols: Dissolution tests were performed in ACSF (117 mM NaCl, 2 mM KCl, 1.25 mM KH_2PO_4, 1 mM $MgSO_4$, 2 mM $CaCl_2$, 25 mM D-glucose, 26 mM $NaHCO_3$, 1 mM L-ascorbic acid, pH 7.4). Additional tests were also performed on PBS (Sigma Aldrich Product No. 806 552). These protocols were performed under body temperature conditions, placing the solutions in a water bath at 37 °C. The flexible neural probes with their respective coatings were submerged in the solution for 25 min, taking microscope images before submersion, and at the 5-, 15-, and 25 min marks. Regarding the quantitative analysis, 5 mm diameter HD4110 disks were fabricated, following the same protocol as the flexible neural probes, and coated with each of the bioresorbable stiffeners as well as methylene blue to aid in the visualization of the degradation process. These were then immersed in ACSF at body temperature, and the percentage area dissolved over time was quantified using video imaging.

70% ethanol (Sigma-Aldrich CAS 64-17-5) was used as the second dissolution protocol to test a possible sterilization method for the flexible neural probes. All probes with their respective coatings were submerged in 70% ethanol at room temperature for 30 min. Images of the coatings were obtained before and after the procedure to evaluate the suitability of this sterilization protocol.

All optical microscopy was performed using an Olympus BX51 with an Olympus UC30 Lens and the cellSens Standard Software for visualization.

Probe Implantation: Sprague–Dawley rats were implanted bilaterally in the ventral Cornu Ammonis 3 (CA3) area at stereotaxic coordinates anteroposterior −5.5 mm, mediolateral −4.5 mm, and dorsoventral −5.8 mm according to the Rat Brain Atlas.[66] Rats were anesthetized with isoflurane (4% induction, 1.5–2% mask connected to Kopf stereotaxic frame, flow rate 1.5 L min^{-1}) and injected with anti-inflammatory drug (Carprofen 5 mg kg^{-1}, s.c.) to reduce animal discomfort. The skin was disinfected and cut to expose the skull, then craniotomies were performed using a microdrill. Surgical tools and dummy probes were previously sterilized in 70% ethanol for 30 min or under UV light for 40 min. Probes were then fixed to the stereotaxic arm using an inserter tool (ATLAS Neuroengineering, Belgium) connected to a vacuum pump. Dummy probes were inserted one for each hemisphere to reduce the number of animals, fixed in position with cyanoacrylate and dental cement, and the rat head was sutured. Anti-inflammatory (Carprofen 5 mg kg^{-1}, s.c.) and antibiotic (Enrofloxacin 5 mg kg^{-1}, s.c.) drugs were administered to reduce postsurgical pain and risk of infection, and saline (NaCl 0.9%, 0.5 mL, s.c.) was injected to rehydrate the rat. Topically, an anesthetic and antimicrobial gel (Lidocaine 2.50 g, Neomycin 0.50 g, Fluocinolone 0.025 g) was applied on the suture line. The animal was

monitored until full recovery from the anesthesia, and the pain level was scored for the following 3 days using the rat Grimace scale.[67]

Histology/Immunohistochemistry: Ten days after the surgery, rats were euthanized under anesthesia and intracardially perfused with saline followed by cold fixative 4% paraformaldehyde (PFA) in PBS. Brains were then collected, put in a vial with the fixative solution, stored at 4 °C for 24 h, and then transferred into a 30% sucrose solution for at least 48 h, then frozen at −80 °C and sliced with the cryostat. The coronal brain sections were mounted on glass slides, left to dry, and stained with hematoxylin and eosin (H&E) staining for histological observation. To perform the H&E staining, slides were submerged in PBS, then in Mayer's hematoxylin (0.1%), and then rinsed in Milli-Q water before being soaked in Eosin solution. The slides were rinsed in Milli-Q and dipped in ethanol at increasing concentrations, 50%, 70%, 90%, and 100%. Finally, the slides were dipped in xylene, mounted with Eukitt and cover glass, and left to dry overnight.

Brain slice images were acquired using the Eclipse Ci-L upright microscope (Nikon Instruments, USA) and acquired using NIS-Elements D software (Nikon Instruments, USA).

Statistical Analysis: For the mechanical characterization and dissolution studies, at least three samples were tested for each of the bioresorbable coatings, with studies repeated on different sample preparations obtained in different days to validate the results. The results are presented as the mean $\pm$SD (standard deviation), both in the main text and in the supplementary information. For the chemical characterization and preliminary in vivo studies, at least two samples were tested for each of the relevant bioresorbable coatings. One-way ANOVA followed by post-hoc Tukey test was performed using Origin 2019b; p values < 0.05 were considered to be statistically significant.

Supporting Information

Supporting Information is available from the Wiley Online Library or from the author.

Acknowledgements

Conflict of Interest

The authors declare no conflict of interest.

Data Availability Statement

The data that support the findings of this study are available in the supplementary material of this article.

Keywords

[1] R. Bartholow, *Am. J. Med. Sci.* **1874**, *134*, 305.
[2] J. Orbach, D. J. Ehrlich, *Arch. Gen. Psychiatry* **1962**, *7*, 223.
[3] A. L. Benabid, P. Pollak, D. Hoffmann, C. Gervason, M. Hommel, J. E. Perret, J. de Rougemont, D. M. Gao, *Lancet* **1991**, *337*, 403.
[4] A. L. Benabid, P. Pollak, D. Gao, D. Hoffmann, P. Limousin, E. Gay, I. Payen, A. Benazzouz, *J. Neurosurg.* **1996**, *84*, 203.
[5] K. D. Wise, J. B. Angell, A. Starr, *IEEE Trans. Biomed. Eng.* **1970**, *BME-17*, 238.
[6] E. McGlynn, V. Nabaei, E. Ren, G. Galeote-Checa, R. Das, G. Curia, H. Heidari, *Adv. Sci.* **2021**, *8*, 2002693.
[7] K. E. Jones, P. K. Campbell, R. A. Normann, *Ann. Biomed. Eng.* **1992**, *20*, 423.
[8] M. Velliste, S. Perel, M. C. Spalding, A. S. Whitford, A. B. Schwartz, *Nature* **2008**, *453*, 1098.
[9] M. Capogrosso, T. Milekovic, D. Borton, F. Wagner, E. M. Moraud, J. B. Mignardot, N. Buse, J. Gandar, Q. Barraud, D. Xing, E. Rey, S. Duis, Y. Jianzhong, W. K. D. Ko, Q. Li, P. Detemple, T. Denison, S. Micera, E. Bezard, J. Bloch, G. Courtine, *Nature* **2016**, *539*, 284.
[10] J. D. Simeral, S. P. Kim, M. J. Black, J. P. Donoghue, L. R. Hochberg, *J. Neural Eng.* **2011**, *8*, 025027.
[11] E. Patrick, M. E. Orazem, J. C. Sanchez, T. Nishida, *J. Neurosci. Methods* **2011**, *198*, 158.
[12] L. A. Geddes, R. Roeder, *Ann. Biomed. Eng.* **2003**, *31*, 879.
[13] E. Axpe, G. Orive, K. Franze, E. A. Appel, *Nat. Commun.* **2020**, *11*, 3423.
[14] S. Budday, G. Sommer, G. A. Holzapfel, P. Steinmann, E. Kuhl, *J. Mech. Behav. Biomed. Mater.* **2017**, *74*, 463.
[15] K. Scholten, C. E. Larson, H. Xu, D. Song, E. Meng, *J. Microelectromech. Syst.* **2020**, *29*, 1054.
[16] P. J. Rousche, D. S. Pellinen, D. P. Pivin, J. C. Williams, R. J. Vetter, D. R. Kipke, *IEEE Trans. Biomed. Eng.* **2001**, *48*, 361.
[17] D. A. Soscia, D. Lam, A. C. Tooker, H. A. Enright, M. Triplett, P. Karande, S. K. G. Peters, A. P. Sales, E. K. Wheeler, N. O. Fischer, *Lab Chip* **2020**, *20*, 901.
[18] A. Weltman, J. Yoo, E. Meng, *Micromachines* **2016**, *7*, 180.
[19] A. A. Sharp, H. V. Panchawagh, A. Ortega, R. Artale, S. Richardson-Burns, D. S. Finch, K. Gall, R. L. Mahajan, D. Restrepo, *J. Neural Eng.* **2006**, *3*, L23.
[20] A. J. Shoffstall, S. Srinivasan, M. Willis, A. M. Stiller, M. Ecker, W. E. Voit, J. J. Pancrazio, J. R. Capadona, *Sci. Rep.* **2018**, *8*, 122.
[21] S. L. Bourke, J. Kohn, *Adv. Drug Delivery Rev.* **2003**, *55*, 447.
[22] R. Boni, A. Ali, A. Shavandi, A. N. Clarkson, *J. Biomed. Sci.* **2018**, *25*, 90.
[23] F. Wu, M. Im, E. Yoon, in *2011 16th Inter. Solid-State Sensors, Actuators and Microsystems Conf.*, IEEE, Beijing, China **2011**, pp. 966–969.
[24] Y. Cao, B. Wang, *Int. J. Mol. Sci.* **2009**, *10*, 1514.
[25] X. Hu, K. Shmelev, L. Sun, E. S. Gil, S. H. Park, P. Cebe, D. L. Kaplan, *Biomacromolecules* **2011**, *12*, 1686.
[26] Q. Lu, X. Hu, X. Wang, J. A. Kluge, S. Lu, P. Cebe, D. L. Kaplan, *Acta Biomater.* **2010**, *6*, 1380.
[27] A. Lecomte, V. Castagnola, E. Descamps, L. Dahan, M. C. Blatché, T. M. Dinis, E. Leclerc, C. Egles, C. Bergaud, *J. Micromech. Microeng.* **2015**, *25*, 125003.
[28] C. Vepari, D. L. Kaplan, *Prog. Polym. Sci.* **2007**, *32*, 991.
[29] L. W. Tien, F. Wu, M. D. Tang-Schomer, E. Yoon, F. G. Omenetto, D. L. Kaplan, *Adv. Funct. Mater.* **2013**, *23*, 3185.

[30] C. Metallo, B. A. Trimmer, *J. Biol. Methods* **2015**, *2*, e13.

[31] H. J. Jin, J. Park, V. Karageorgiou, U. J. Kim, R. Valluzzi, P. Cebe, D. L. Kaplan, *Adv. Funct. Mater.* **2005**, *15*, 1241.

[32] A. Singh, H. Zhu, J. He, in *Annual Inter. Conf. of the IEEE Engineering in Medicine and Biology - Proceedings*, IEEE, San Francisco, CA **2004**, pp. 4298–4301.

[33] M. Jeon, J. Cho, Y. K. Kim, D. Jung, E. S. Yoon, S. Shin, I. J. Cho, *J. Micromech. Microeng.* **2014**, *24*, 025010.

[34] C. Hassler, T. Boretius, T. Stieglitz, *J. Polym. Sci., Part B: Polym. Phys.* **2011**, *49*, 18.

[35] Z. Xiang, S. C. Yen, N. Xue, T. Sun, W. M. Tsang, S. Zhang, L. de Liao, N. V. Thakor, C. Lee, *J. Micromech. Microeng.* **2014**, *24*, 065015.

[36] G. Palazzolo, N. Broguiere, O. Cenciarelli, H. Dermutz, M. Zenobi-Wong, *Tissue Eng. Part A* **2015**, *21*, 2177.

[37] L. Ferlauto, A. N. D'Angelo, P. Vagni, M. J. I. A. Leccardi, F. M. Mor, E. A. Cuttaz, M. O. Heuschkel, L. Stoppini, D. Ghezzi, *Front. Neurosci.* **2018**, *12*, 648.

[38] A. Sridharan, J. Muthuswamy, *Micromachines* **2021**, *12*, 761.

[39] C. Tang, S. Xie, M. Wang, J. Feng, Z. Han, X. Wu, L. Wang, C. Chen, J. Wang, L. Jiang, P. Chen, X. Sun, H. Peng, *J. Mater. Chem. B* **2020**, *8*, 4387.

[40] S. Park, H. Yuk, R. Zhao, Y. S. Yim, E. W. Woldeghebriel, J. Kang, A. Canales, Y. Fink, G. B. Choi, X. Zhao, P. Anikeeva, *Nat. Commun.* **2021**, *12*, 3435.

[41] T. T. Nguyen, J. Ratanavaraporn, S. Yodmuang, in *BMEiCON 2019 - 12th Biomedical Engineering Inter. Conf.*, IEEE, Ubon Ratchathani, Thailand **2019**, https://doi.org/10.1109/BMEICON47515.2019.8990292.

[42] W. Jensen, U. G. Hofmann, K. Yoshida, in *Annual Inter. Conf. of the IEEE Engineering in Medicine and Biology – Proceedings*, Vol. 3, IEEE, Cancun, Mexico **2003**, p. 2168.

[43] M. Cen-Puc, A. Schander, M. G. Vargasgleason, W. Lang, *Polymers* **2021**, *13*, 1955.

[44] T. Matsumoto, M. Kawai, T. Masuda, *Biorheology* **1992**, *29*, 411.

[45] H. Hecht, S. Srebnik, *Biomacromolecules* **2016**, *17*, 2160.

[46] S. Lopes, L. Bueno, F. de Aguiar Júnior, C. L. L. Finkler, *An. Acad. Bras. Cienc.* **2017**, *89*, 1601.

[47] K. Sakugawa, A. Ikeda, A. Takemura, H. Ono, *J. Appl. Polym. Sci.* **2004**, *93*, 1372.

[48] Y. Wang, B. J. Kim, B. Peng, W. Li, Y. Wang, M. Li, F. G. Omenetto, *Proc. Natl. Acad. Sci. U S A* **2019**, *116*, 21361.

[49] P. Cebe, X. Hu, D. L. Kaplan, E. Zhuravlev, A. Wurm, D. Arbeiter, C. Schick, *Sci. Rep.* **2013**, *3*, 1130.

[50] T. Hashimoto, Y. Nakamura, Y. Tamada, H. Kurosu, T. Kameda, *PeerJ Mater. Sci.* **2020**, *2*, e8.

[51] Y. Kambe, Y. Mizoguchi, K. Kuwahara, T. Nakaoki, Y. Hirano, T. Yamaoka, *Polym. Degrad. Stab.* **2020**, *179*, 109240.

[52] J. Wang, M. M. Kliks, S. Jun, M. Jackson, Q. X. Li, *J. Food Sci.* **2010**, *75*, C208.

[53] C. Narita, Y. Okahisa, I. Wataoka, K. Yamada, *ACS Omega* **2020**, *5*, 22786.

[54] H. Y. Wang, Y. Q. Zhang, *Sci. Rep.* **2014**, *4*, 6182.

[55] D. V. S. K. Gunapu, Y. B. Prasad, V. S. Mudigunda, P. Yasam, A. K. Rengan, R. Korla, S. R. K. Vanjari, *Int. J. Biol. Macromol.* **2021**, *176*, 498.

[56] T. Asakura, *Molecules* **2021**, *26*, 3706.

[57] S. H. Felix, K. G. Shah, V. M. Tolosa, H. J. Sheth, A. C. Tooker, T. L. Delima, S. P. Jadhav, L. M. Frank, S. S. Pannu, *J. Visualized Exp.* **2013**, *79*, e50609.

[58] C. Cointe, A. Laborde, L. G. Nowak, D. N. Arvanitis, D. Bourrier, C. Bergaud, A. Maziz, *Microsyst. Nanoeng.* **2022**, *8*, 21.

[59] A. Baldwin, L. Yu, E. Meng, *J. Microelectromech. Syst.* **2016**, *25*, 1015.

[60] D. O. de Lima, C. G. Aimoli, M. M. Beppu, *Mater. Sci. Eng., C* **2009**, *29*, 1109.

[61] D. O. de Lima, M. H. P. da Silva, J. B. de Campos, A. M. Rossi, M. M. Beppu, *Key Eng. Mater.* **2006**, *309–311 I*, 195.

[62] K. Y. Lee, D. J. Mooney, *Prog. Polym. Sci.* **2012**, *37*, 106.

[63] C. Stylianopoulos, *Encycl. Hum. Nutr.* **2013**, *1–4*, 265.

[64] F. Wu, L. Tien, F. Chen, D. Kaplan, J. Berke, E. Yoon, in *2013 Transducers and Eurosensors XXVII: The 17th Inter. Conf. on Solid-State Sensors, Actuators and Microsystems, Transducers and Eurosensors 2013*, IEEE, Barcelona, Spain **2013**, p. 888.

[65] W. Zhang, X. Zhou, Y. He, L. Xu, J. Xie, *Biomed. Microdevices* **2021**, *23*, 17.

[66] G. Paxinos, C. Watson, *The Rat Brain In Stereotaxic Coordinates: Hard Cover Edition*, Academic Press (imprint of Elsevier), London **2013**.

[67] S. G. Sotocinal, R. E. Sorge, A. Zaloum, A. H. Tuttle, L. J. Martin, J. S. Wieskopf, J. C. S. Mapplebeck, P. Wei, S. Zhan, S. Zhang, J. J. McDougall, O. D. King, J. S. Mogil, *Mol. Pain* **2011**, *7*, 1744.